OPEN

NPG Asia Materials (2014) 6, e80; doi:10.1038/am.2013.69

www.nature.com/am

REVIEW

Cellulose nanocrystal-based materials: from liquid crystal self-assembly and glass formation to multifunctional thin films

Jan PF Lagerwall[1,2], Christina Schütz[3,4], Michaela Salajkova[4,5], JungHyun Noh[1], Ji Hyun Park[1], Giusy Scalia[1,2] and Lennart Bergström[3]

Cellulose nanocrystals (CNCs), produced by the acid hydrolysis of wood, cotton or other cellulose-rich sources, constitute a renewable nanosized raw material with a broad range of envisaged uses: for example, in composites, cosmetics and medical devices. The intriguing ability of CNCs to self-organize into a chiral nematic (cholesteric) liquid crystal phase with a helical arrangement has attracted significant interest, resulting in much research effort, as this arrangement gives dried CNC films a photonic band gap. The films thus acquire attractive optical properties, creating possibilities for use in applications such as security papers and mirrorless lasing. In this critical review, we discuss the sensitive balance between glass formation and liquid crystal self-assembly that governs the formation of the desired helical structure. We show that several as yet unclarified observations—some constituting severe obstacles for applications of CNCs—may result from competition between the two phenomena. Moreover, by comparison with the corresponding self-assembly processes of other rod-like nanoparticles, for example, carbon nanotubes and *fd* virus particles, we outline how further liquid crystal ordering phenomena may be expected from CNCs if the suspension parameters can be better controlled. Alternative interpretations of some unexpected phenomena are provided, and topics for future research are identified, as are new potential application strategies.
NPG Asia Materials (2014) **6,** e80; doi:10.1038/am.2013.69; published online 10 January 2014

Keywords: cholesteric; gel; glass; liquid crystal; nanocellulose; photonic crystal; self-assembly

INTRODUCTION

Nanomaterials based on renewable resources are attracting rapidly growing interest, both from a fundamental scientific point of view and from the perspective of developing novel structural and functional macroscopic materials.[1,2] Using nature-based nanomaterials offers ecological advantages, and the extraordinary mechanical performance and/or photonic crystal character of biological composites such as bone, nacre, wood, beetle scales and butterfly wings is also an important inspiration for the development of new multifunctional materials.[3–5] However, full utilization of the intrinsic properties of nanosized starting materials requires the development of robust and versatile synthetic and processing routes to control assembly over several length scales.[6–8]

Cellulose, one of the most versatile and widely found biopolymers in nature, has been used by humans for millennia as a building material, an energy source, a component of clothing and for storing and sharing knowledge and culture. Today, cellulose materials are used in a wide range of applications, and the paper and pulp industry constitutes a significant share of the economic output in many countries. One recent strong trend, on an international scale, is to focus on the isolation of fibrils and whiskers of cellulose with diameters in the nanometer range and to utilize their enhanced properties to develop novel cellulose-based materials with diverse advanced functionalities. Various forms of such nanocellulose can be produced by different routes and from a variety of cellulose sources, as summarized in a series of recent reviews focusing on the production, chemistry and current application strategies of cellulose nanocrystals (CNCs), microfibrillated cellulose and bacterial nanocellulose.[9–13] Nanocellulose features an attractive combination of properties such as biocompatibility, a high elastic modulus (similar to steel), a low thermal expansion coefficient, optical transparency and anisotropy, negative diamagnetic anisotropy and flexible surface chemistry, making it of interest in applications such as composites,[14] security papers,[15] wound dressings and medical implants.[16,17] Two representative examples of application strategies that are being pursued are shown in Figure 1.

[1]Nano Science and Technology Program, Graduate School of Convergence Science and Technology, Seoul National University, Suwon, Korea; [2]Advanced Institute of Convergence Technologies, Suwon, Korea; [3]Stockholm University, Department of Materials and Environmental Chemistry, Stockholm, Sweden; [4]Wallenberg Wood Science Centre, Stockholm, Sweden and [5]Department of Fiber and Polymer Technology, Royal Institute of Technology, Stockholm, Sweden
Correspondence: Professor JPF Lagerwall, Nano Science and Technology Program, Graduate School of Convergence Science and Technology, Seoul National University, 864-1 Iui-dong, Suwon-si, Gyeonggi-do 443-270, Korea or L Bergström, Stockholm University, Department of Materials and Environmental Chemistry, Stockholm 106 91, Sweden.
E-mail: jan.lagerwall@lcsoftmatter.com or lennart.bergstrom@mmk.su.se
Received 9 August 2013; revised 24 September 2013; accepted 8 October 2013

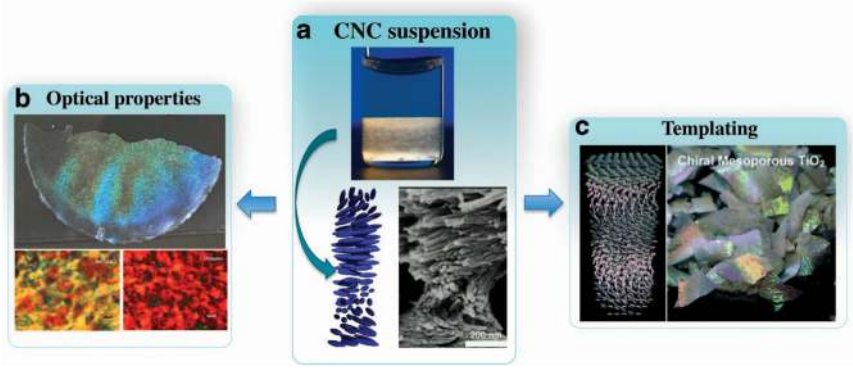

Figure 1 Graphical overview of the characteristics and current utilization of CNC chiral nematic phases with helical nanorod arrangement. (**a**) Shows the formation of a chiral nematic liquid crystal phase and its coexistence with an isotropic phase in a CNC suspension of 5 wt% (upper image). The helical arrangement of the nanorods is illustrated schematically next to a scanning electron microscopy image of an actual CNC helix (reproduced with permission from Majoinen *et al.*,[29] Copyright © 2012, Springer). Currently explored utilization schemes are exemplified by (**b**) the iridescence revealing the photonic crystal character of the film (reproduced with permission from Zhang *et al.*,[15] Copyright © 2012, SPIE) and (**c**) templating of the CNC-derived helical structure into inorganic materials (here, titanium dioxide) (reproduced with permission from Shopsowitz *et al.*[84] Copyright © 2012 WILEY-VCH Verlag GmbH & Co. KGaA, Weinheim).

A milestone in the development of nanocellulose science and technology was the discovery by Gray and co-workers[18] that suspensions of stiff and rod-like CNCs, derived from natural cellulose sources via acid hydrolysis, can form a stable chiral nematic liquid crystalline phase. The chiral nematic—also called cholesteric—phase is characterized by long-range orientational order of the nanorods combined with a helical modulation of the direction in which they align[19,20] (see Supplementary Box 1 for more details). The local alignment orientation is referred to as the *director*. In the fluid state, the pitch of this helical modulation is typically in the range of tens of micrometers, but upon drying, it frequently is reduced to submicrometer values, resulting in Bragg reflection of visible light from dried films, that is, the material acquires a photonic band gap with a consequent striking iridescent color. The attractive optical properties of this self-assembled bio-derived photonic crystal have inspired several attempts to utilize CNC films in novel applications such as optical encryption[15] or as chiral templates.[21]

It has also recently been recognized that the extraordinarily high fracture toughness of the mineralized tissues of many marine organisms, for example, the cuticle of lobster[22] and the extremely damage-tolerant dactyl club of stomatopods,[5] is related to the dissipation of the fracture energy by the helical organization of the fibrillar chitin matrix, another important rod-like polysaccharide. Weaver *et al.*[5] combined synchrotron diffraction texture analysis, micromechanical measurements and dynamic finite element modeling to show that the expanded helical architecture of chitin fibers with a pitch of 75 μm provides several toughening mechanisms that hinder the catastrophic propagation of cracks. These recent advances build upon the seminal work of Bouligand and co-workers,[23–27] who were the first to recognize that many natural high-performance biocomposite materials have structures resulting from liquid crystalline self-assembly.

Controlling and understanding the liquid crystalline self-assembly and the resulting helical ordering of CNCs are thus goals of fundamental importance but they are also steps along a route to produce novel materials with desirable optical and mechanical properties. Compared with photonic crystals formed via non-liquid crystalline self-assembly of spherical colloidal particles,[28] the helical liquid crystalline self-assembly of rod-like CNC particles leads to a more complex internal structure, rendering the material chiral and adding sensitivity to circular polarization while, at the same time, dramatically enhancing the mechanical properties.[22] However, progress in this area is hampered by a number of important phenomena that remain unexplained, as well as a few controversies regarding the self-organization of CNCs. For instance, the notion that the reflected color is due to a photonic bandgap resulting from the helical structure has been challenged based on observations of a helix that is too long for Bragg reflection to take place in the visible wavelength range,[29] and a surprising dependence on the ionic strength of the phase sequence and helical pitch has been observed in some systems.[30] One of the aims of this critical review is to emphasize the physics and physical chemistry-related issues involved in CNC self-assembly by comparing it with similar processes in suspensions of other nanorod classes. This approach gives an important additional perspective that is complementary to the current state of understanding, and we believe it can be very beneficial for the future development of the field and the realization of CNC-based functional materials. We focus particularly on the macroscopic phase behavior and the balance between liquid crystalline ordering and a transition into a gel-like glassy state.

Although an increasing particle concentration in a colloid of rod-like particles can lead to nematic or higher-ordered liquid crystal phases (smectic and columnar, see Supplementary Box 1), it also considerably enhances the probability of close rod encounters. For long and slender rods, such encounters can eventually induce a phenomenon referred to as rigidity percolation, or physical gelation, that is, the particles block each others' movements to such an extent that no further reorganization is possible.[31] As a result, the fluid phase turns into a gel-like glass, with whatever order or disorder that prevailed before the glass transition made permanent. For single-wall carbon nanotubes, such kinetic arrest has been experimentally determined to take place directly from the isotropic liquid state at the extremely low rod volume fraction of ~ 0.003.[32] Here, the high length polydispersity and extreme aspect ratio of carbon nanotubes have important roles in triggering the glass transition before any liquid crystalline ordering. Although the corresponding gelation phenomenon of CNCs (typically occurring at higher particle concentrations) is well-known, its consequences on the liquid crystal behavior and the structure that is finally obtained in dried samples has thus far not been discussed.

In this review, we compare observations of the macroscopic phase behavior of CNC suspensions with reports on other relevant rod-particle colloids, specifically filamentous viruses (bacteriophages), goethite mineral nanorods and carbon nanotube suspensions (see Figure 2 for representative pictures). We limit ourselves to studies involving aqueous liquid crystalline suspensions of CNCs and do not discuss suspensions of microfibrillated cellulose. Revisiting and reanalyzing some previously published results, among them the examples mentioned above, we are able to propose explanations for some poorly understood but important phenomena by explicitly considering the sensitive balance between liquid crystalline ordering and glass transition as the CNC concentration and ionic strength are varied. We conclude by discussing how an improved understanding of the self-organization phenomena in CNC suspensions, in particular during the drying phase, can allow the development of novel, valuable materials and as yet unconsidered applications of CNC-derived composites that take advantage of the unique mechanical and optical properties arising from the helical arrangement of the nanorods over macroscopic distances.

EXTRACTION OF CNCs FROM BIOLOGICAL SOURCES

Cellulose on its smallest scale occurs naturally in the form of an elementary fibril, regardless of the source.[11,13] Nanoparticles are extracted from a raw cellulose sample following two main steps: the first is the purification and homogenization pretreatment of the source material to allow uniform reaction conditions, and the second is the separation of the purified cellulose material into its microfibrillar and/or nanocrystalline components.

The purification and homogenization steps are adapted based on the cellulose source. For wood and plants, the most important step is the removal of the matrix materials hemicellulose and lignin.[33] The second step, separation into microfibrillar or nanocrystalline components, can be performed by enzymatic hydrolysis, mechanical treatment or acid hydrolysis.[10,33,34] The predominant method for isolating CNCs from cellulose fibers is based on acid hydrolysis, a technique that dates back to the seminal studies by Rånby,[35] with a number of more recent refinements. Table 1 summarizes the characteristic CNCs of different sources that have been isolated by sulfuric acid hydrolysis. If the CNCs are prepared by hydrochloric acid hydrolysis, the hydroxyl groups on the surface remain. The surface is consequently only weakly charged, and the colloidal stability is poor.[36,37] In contrast, sulfuric acid hydrolysis yields CNCs with a charged surface and thus a good colloidal stability in aqueous media.

It was recently shown that carboxylic groups can be introduced, resulting in a higher surface charge compared with sulfuric acid-hydrolyzed CNCs, by using either a pre-[38] or post-[39] treatment with TEMPO (2,2,6,6,-tetramethylpiperidine-1-oxyl)-mediated oxidation in addition to hydrochloric acid hydrolysis. TEMPO selectively oxidizes the primary hydroxy groups (C6) into carboxylates, whereas the secondary hydroxyl groups remain unaffected. Positive charges can also be introduced onto the surface by ammonium-containing groups, for example, epoxypropyltrimethylammonium chloride,[40] by grafting. Figure 3 gives a schematic overview of the typical modifications in the CNC production route and the surface chemistry of the final product.

Table 1 Examples of CNCs isolated from different sources by sulfuric acid hydrolysis

Cellulose origin	*Length (nm)*	*Width (nm)*	*Reference*
Bacteria	100–1000	10–50	52
Cotton	70–300	5–10	52,55,96
Wood	100–300	3–5	36,64,97
Tunicate	500–1000	10–30	80,96,98
Valonia	>1000	10–20	99

Abbreviation: CNCs, cellulose nanocrystals.

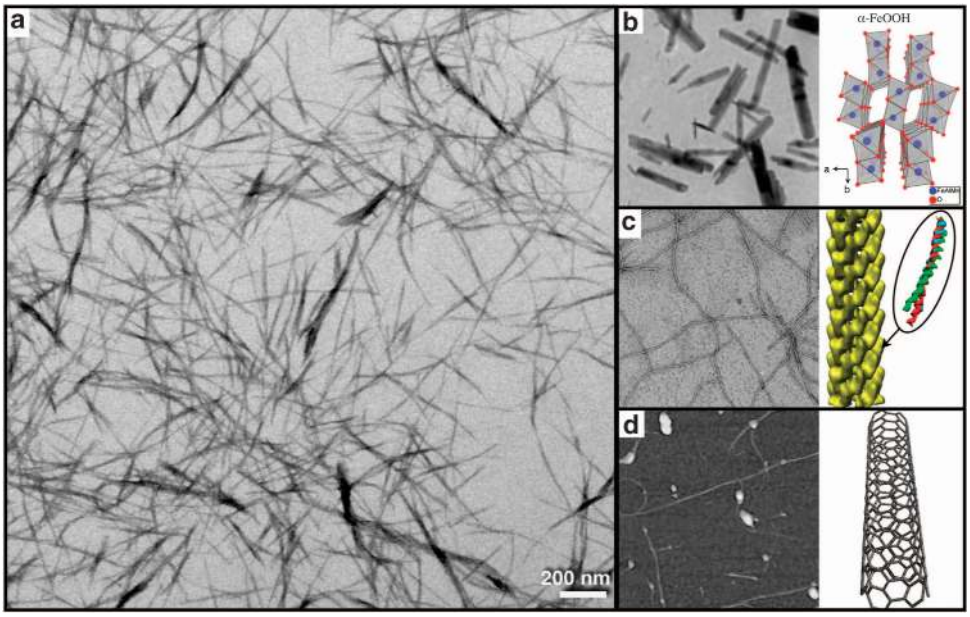

Figure 2 High-magnification images of CNCs (**a**, reproduced with permission from Salajkova *et al.*[38] of The Royal Society of Chemistry), goethite nanorods (**b**, micrograph reproduced with permission from Vroege *et al.*[46] Copyright © 2006 WILEY-VCH Verlag GmbH & Co. KGaA, Weinheim), *fd* virus (**c**, micrograph and drawings reprinted from Wang *et al.*[93] Copyright (2006), with permission from Elsevier) and single-wall carbon nanotubes (**d**, atomic force microscope (AFM) image reproduced with permission from Dolle *et al.*[94] Copyright © 2012 WILEY-VCH Verlag GmbH & Co. KGaA, Weinheim). All images have the same scale (scale bar in **a**).

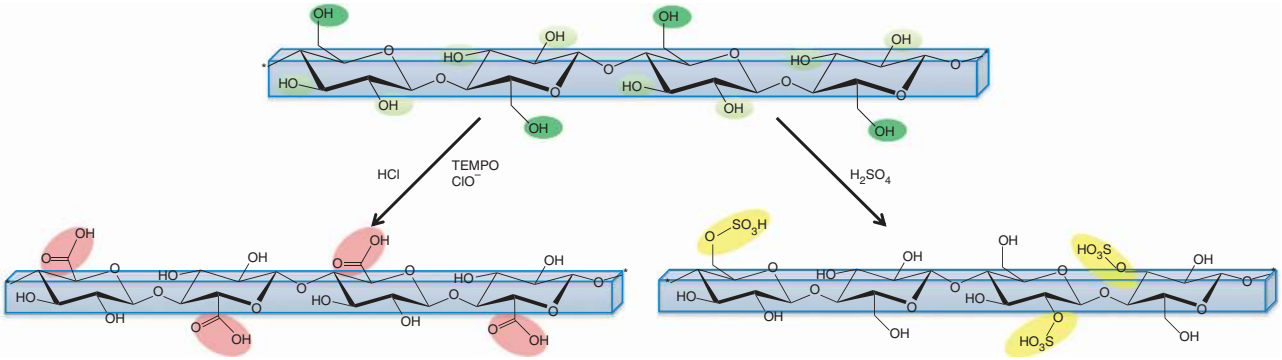

Figure 3 Schematic of the two routes for producing anionic CNCs, resulting in carboxylate (left) and sulfate half ester (right) surface groups.

PHASE DIAGRAMS OF CELLULOSE NANOCRYSTAL SUSPENSIONS

The high aspect ratio of CNC rods promotes the formation of liquid crystalline phases (see Supplementary Box 1), as well as arrested gel-like glassy states. In fact, both phenomena are typically encountered as the concentration of colloidally stable rod-like particles is increased, with one or several liquid crystalline phases normally developing first[41,42] and with the glass transition taking place at a somewhat higher concentration. It is instructive to compare the behavior of CNC suspensions at different concentrations with that of other rod-shaped particle colloids.

The phase behavior of suspensions of rod-shaped bacteriophage viruses, in particular the *fd* virus,[43–45] and of goethite nanorods[46] has been studied in detail. The former are examples *par excellence* of monodisperse colloids (the viruses are uniform in length), whereas the latter represents the opposite group of high polydispersity. While rod-like bacteriophages have indeed been found to exhibit cholesteric (they are chiral) and smectic phases,[44,45] Grelet recently found that a columnar liquid crystal and a columnar crystal phase could also develop.[44] Surprisingly, even very polydisperse goethite nanorods could produce a liquid crystal with smectic order,[46] most likely as a result of gravity-driven spontaneous fractionation and consequent phase segregation of these relatively heavy mineral rods.

Carbon nanotubes are challenging to study at higher concentrations owing to the difficulty of preventing particle aggregation, which occurs at a concentration of approximately 1 wt%. Thus, no other liquid crystal phase apart from the nematic phase has been reported thus far,[47–50] and a glass transition was reported only for very well-dispersed carbon nanotubes at a very low threshold concentration.[32] The difficulty in observing higher-order liquid crystal phases with carbon nanotubes is also a result of the large size distribution of the tube length.

The monodispersity of the *fd* virus and similar bacteriophages most likely helps promote the prevalence of ordered phases with respect to the glass transition, but the salt concentration also has an important role. In fact, Kang and Dhont[43] recently reported a direct transition from a cholesteric to a glassy state in studies of *fd* virus suspensions at the low salt limit. At virus concentrations greater than 12 mg ml^{-1}, the nonequilibrium texture imposed in the cholesteric phase by shearing no longer relaxes but rather is vitrified in a glassy state. The authors explain this observation as a result of each virus rod being prevented from conducting any large-scale rearrangement because it finds itself in an electrostatic 'cage' established by the long-range repulsive forces from the charged neighboring particles.

The liquid crystal behavior of CNC dispersions at concentrations above 10–15 wt% is largely unexplored, *cf.* Figure 4, most likely because the glass transition makes it difficult to study equilibrium phases at high particle concentrations. We believe that the glassy state is a key component in explaining the absence of observed high-order liquid crystal phases and the great variety of structural features found in films formed by drying CNC suspensions. Indeed, if the glass transition could be suppressed or at least shifted to a higher concentration, a transition into a columnar liquid crystal phase would be expected in CNC suspensions.

In what follows, we survey some key studies performed on CNCs of different origins and thus different aspect ratios (most notably plant-derived versus bacterial CNCs), at different rod concentrations and varying ionic strength *I*. Taking as a starting point the Onsager model[51] (see Supplementary Box 1), which predicts that the required volume fraction for liquid crystal formation is inversely proportional to the rod aspect ratio, the onset concentration of liquid crystallinity is expected to decrease if the rod-like CNC is longer and thinner. Indeed, dispersions of bacterial CNCs, with lengths on the order of 1–2 μm and an aspect ratio in the range of 50–100,[30,52] show nematic ordering well below 1 wt% CNC, *cf.* Figure 4. With CNCs derived from fresh wood, the onset concentration is found at ~2 wt%, and when filter paper is used as the CNC source, the onset concentration increases to ~5 wt%, reflecting the lower aspect ratios of these CNCs of ~20–50[10,38,53] and 15–40,[54,55] respectively, as well as their lower average lengths (in the range of 100–300 nm). As CNC samples are highly polydisperse, the influence of the aspect ratio can be recognized even when using a single CNC source. Hirai *et al.*[30] and Dong *et al.*[54] confirmed a fractionation of longer CNC rods into the anisotropic phase and of shorter rods into the isotropic fraction.

For increasing CNC concentrations, the Onsager model predicts a linear increase of the volume fraction of the nematic phase throughout the biphasic regime until the sample is fully liquid crystalline. This behavior is found only for the very highest aspect ratio bacterial CNC, which also has a comparatively low surface charge. For the wood-derived CNC, the volume fraction curve always levels off, and a higher CNC concentration is required to reach complete liquid crystallinity compared with the model prediction, *cf.* Figure 4. Moreover, the absolute CNC concentrations for the onset and saturation of nematic phase formation are approximately one order of magnitude smaller than predicted. For aspect ratios of 100 and 50, the Onsager onset concentrations are 3 and 7 vol.%, respectively, and the saturation concentrations are 5 and 9 vol.%, respectively. These observations demonstrate that, although the Onsager model in its original form contains the relevant physics, it cannot fully describe the liquid crystal formation in CNC suspensions quantitatively.

We may explain the lower than expected threshold concentrations by including the electrostatic repulsion (not accounted for by

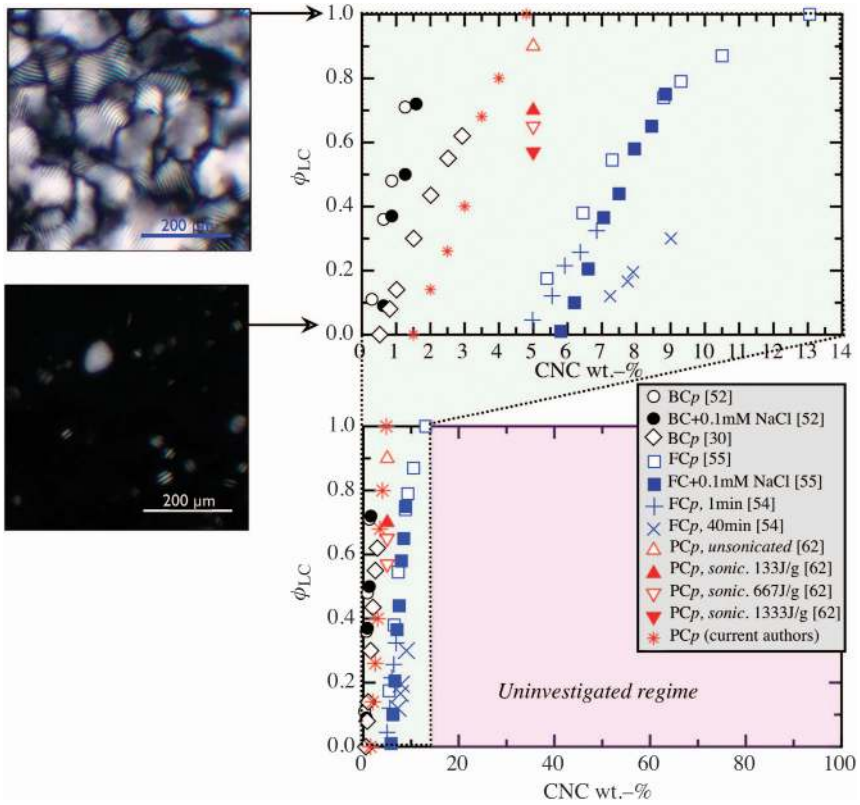

Figure 4 Phase behavior of suspensions of CNCs of different origins, following various treatments or using different additives, together with representative polarizing microscopy texture examples of a fully cholesteric sample (top) and a sample with a tiny liquid crystal fraction coexisting as bright striped droplets with a black isotropic majority phase (bottom). The volume fraction ϕ_{LC} of the liquid crystal phase is plotted as a function of the CNC concentration, zoomed in on the investigated regime in the top diagram. The black data points are obtained with CNCs from bacterial cellulose (BC), blue with filter paper-derived CNCs (FC) and red with fresh wood pulp-derived CNCs (PC). The suffix *p* indicates pure CNCs, without any additive. The source of each data set is specified in the legend. The times indicated for the reference [54] series refer to the duration of sonication.

Onsager) between the charged CNC particles, as this increases the effective CNC volume fraction.[56] Moreover, because the thickness of the electric double layer (given by the Debye screening length κ^{-1}) depends on the ionic strength *I*, and the CNC rods themselves bring counter ions into solution, the effective rod shape and size will change with the CNC concentration. This dependence can explain the nonlinear leveling off of the liquid crystalline volume fraction curve as a function of concentration that is observed for most CNC types, as shown in Figure 4. The effect is weaker for CNCs with a lower surface charge and with a smaller onset concentration for liquid crystalline ordering; hence, the nonlinearity becomes negligible for bacterial CNCs, which are approximately one order of magnitude longer, with ~1/20 of the surface charge of wood-derived CNCs.[30,52]

Dong *et al.*[55] conducted an elegant experiment to demonstrate the influence of the CNC counter ions on the formation of the liquid crystal phase. By adding HCl at varying concentrations to a series of CNC suspensions within the biphasic regime, such that each suspension had a constant pH of 1.61, they effectively canceled out the effect of the counter ions introduced by the cellulose nanorods. Indeed, the anisotropic volume fraction curve then followed a linear dependence on the CNC concentration, as expected from Onsager theory. The impact of the electrostatic repulsion between the rods was further demonstrated by other experiments, where additional salt was introduced to CNC suspensions, increasing the required amount of CNC for liquid crystallinity. Some examples are included in Figure 4. We finally note that electrostatic repulsion also influences the directional interactions between the CNC rods, with an additional term promoting the perpendicular orientation of adjacent rods (this maximizes the distance between individual charges).[57] This influence should have an effect not only on liquid crystal formation in general but also on the pitch of the cholesteric helix.

Hirai *et al.*[30] observed an interesting and rather peculiar reversal in phase behavior in their study of bacterial CNC with added NaCl. Although the volume fraction of the cholesteric phase initially decreased with added salt, as expected, it started increasing again at concentrations greater than 0.75 mM NaCl. The entire CNC suspension was anisotropic at 2 mM NaCl, and because no stripes indicative of a helical structure could be observed, the phase appears to have been chiral nematic with an essentially infinite pitch.

This behavior is truly surprising. It may be related to what van der Schoot[58] and Turner and Cates[59] refer to as supramolecular polymerization in lyotropic liquid crystals. Bacterial cellulose has the highest aspect ratio among CNCs, with some rods reaching several microns in length. Their surface charge density is comparatively low; hence, the addition of NaCl will screen out the electrostatic repulsion to a greater extent than for sulfated CNCs derived from wood pulp or filter paper. Therefore, beyond a critical ionic strength, the repulsion may become so weak that the CNC rods start aggregating. Because this happens in a phase that is nematic, with long-range orientational order but no positional order, the attraction will produce rod-like aggregates that are longer but not much wider than the original rods. As Turner and Cates[59] predicted theoretically, and as was recently

demonstrated experimentally for a micellar nematic phase doped with carbon nanotubes,[60] a positive feedback loop between increasing orientational order and growing rod length can arise in this situation, promoting an increase in the fraction of liquid crystalline order.

HELICAL STRUCTURES IN THE CHIRAL NEMATIC PHASE AND IN DRIED FILMS

The striking ability of CNC suspensions to form self-assembled helical structures that are still present in solvent-free films produced by drying a sample suggests the potential of CNCs to be utilized in novel materials with attractive photonic and mechanical properties. While the CNC helix is always left-handed, reflecting the intrinsic chirality of crystalline cellulose, the value of the pitch (see Supplementary Box 1) can vary greatly, from less than 1 to 50 μm and beyond. The pitch depends on the quality of the CNC, on the concentration, on the ionic strength of the solution and even on the temperature.[61] Many aspects of helix formation are still poorly understood, limiting our ability to control it and to tune the pitch. In particular, for photonic applications, this limitation is a key challenge that must be addressed. It is important to distinguish between the helical director modulation in liquid crystalline suspensions and helical structures found in dried films. While the former reflects an equilibrium situation (provided there is sufficient equilibration time), the internal structure of a dried film is representative of the conditions prevailing within a domain when it entered the gel-like glassy state. The glass formation is a nonequilibrium process that is difficult to control and there are strong variations from time to time and between different regions.

The helix in liquid crystalline CNC suspensions

The number of systematic reports on helix formation in the liquid crystalline phase of CNCs is still rather small, and the information is largely qualitative, based on a limited set of sample texture images such as that shown in Figure 5a. Indeed, there is a need for studies that investigate helix formation in the fluid state and provide high-resolution data from this regime to complement the more numerous quantitative studies of dried films.[15,62,63]

Studies on CNCs derived from filter paper[55] and from wood pulp,[64] as well as on bacterial CNCs,[30] show that the pitch p generally decreases as the particle concentration c is increased. The same type of concentration dependence of the pitch is observed for *fd* virus suspensions, except at high concentrations, where p increases with increasing c.[65] The latter behavior may be understood as a consequence of the suspension being close to a phase transition into a smectic phase. This phase is incompatible with the twisting of the director into a helix; hence, p must increase (the helix is unwound) as the transition is approached. To the best of our knowledge, no reports of increasing pitch of CNC suspensions with increasing c exist, most likely because all forms of CNC produced to date appear to be too polydisperse to produce smectic phases.

Two principal mechanisms can be considered for explaining the decrease in p as the CNC concentration is increased, both of which may contribute in determining the pitch. First, the helix formation is fundamentally driven by the transfer of the chirality of the molecular cellulose to the macroscopic ordering of the liquid crystal phase. Thus, just as in other cases of chirality transfer in liquid crystals,[20,66] the more chiral species that are present in the system (the larger the CNC content in this case), the stronger the total force for the twisting will be. Second, because the CNC rods are charged, the increasing ionic strength upon increasing the particle concentration will decrease the range of the exponentially decaying electrostatic repulsion and thus allow the rods to approach each other more closely. Although the exact origin of the twisting in lyotropic cholesterics is still a debated issue,[67,68] it is generally accepted that proximity between chiral entities promotes twisting and thus decreases p, whereas an increasing average interparticle distance weakens the twisting force and thus increases the pitch.

The second of these mechanisms is most likely equivalent to a mechanism proposed specifically for the case of CNCs by Araki and Kuga,[52] who also considered the role of ions in solution. Rather than

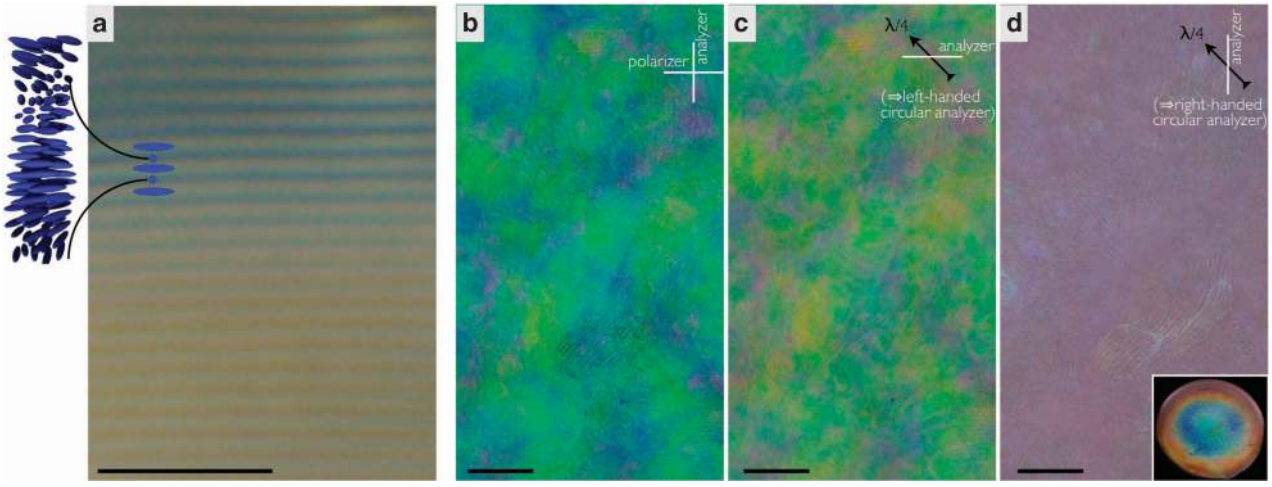

Figure 5 Polarizing microscopy textural traces of CNC helix formation in the liquid crystalline (wet) state (**a**) and in solid CNC samples obtained by drying (**b**–**d**). Scale bars correspond to 50 μm. (**a**) Characteristic regularly spaced helix lines in an aqueous suspension with 5 wt% CNC derived by sulfuric acid hydrolysis of wood pulp, observed in transmission. The distance between two lines is half the pitch ($p/2$), as illustrated in the schematic; hence, the equilibrated helix of this sample has $p \approx 13$ μm. (**b**–**d**) Typical dried film of CNC (same source as above, starting concentration 4.8 wt%) with nonuniform helix orientations and a strong spread in p, observed in reflection. In (**b**), the film is illuminated with linear polarized light and observed through a crossed polarizer (analyzer). In (**c**) and (**d**), it is illuminated with unpolarized light and observed through a λ/4 phase plate followed by the analyzer, together constituting an analyzer for left- (**c**) and right-handed (**d**) circular polarization, respectively. The inset in (**d**) shows the iridescence from a macroscopic, dried CNC film on a circular glass substrate (25 mm in diameter) against a black background, viewed at a slight angle.

considering the average distance between rods, they discussed the impact of electrostatic repulsion on the effective particle shape. Assuming that chiral CNC nanorods have a twisted morphology and that the 'padding' around the rod that is created by the electrostatic repulsion does not fully carry over this twist, they concluded that the effective particle shape loses its chiral character under low salt conditions, where the repulsion is long-range. As the CNC concentration increases, the padding becomes thinner, and the twist of the CNC rod becomes more apparent. However, a thick padding is equivalent to a large average interparticle distance, so it seems that this can be considered a different view of the second mechanism described above.

The impact of electrostatic repulsion, and thus of ionic strength, on the chirality transfer is generally confirmed by studies where inorganic, non-chiral, low molar mass salts are added to suspensions with a constant CNC concentration, thereby tuning the electrostatics without affecting the chirality of the system. Dong *et al.*[55] found a decreasing pitch in filter paper-derived CNC suspensions upon increasing concentration of the added salt, regardless of its type. Slightly more complex is the study on bacterial cellulose by Hirai *et al.*,[30] which was mentioned above. They reported a decreasing pitch upon the addition of NaCl up to 0.75 mM, where the nematic-to-isotropic balance reversed; thereafter, the pitch diverged as more salt was added. The first trend follows the expected behavior found by Dong *et al.*[54] for shorter filter paper-derived CNCs, whereas the second trend can perhaps be understood—if our proposed model for the high salt regime is appropriate—as a result of diverging rod length[64] resulting from a supramolecular polymerization triggered by CNC end-to-end aggregation.

In the study of *fd* virus suspensions by Dogic and Fraden,[65] the reported pitch at a constant virus concentration showed an overall trend of increasing with increasing salt concentration, in contrast to the trend observed with CNCs. One should note, however, that the salt concentrations here were much higher than in the corresponding CNC studies. Moreover, the response of the *fd* virus to salt may involve a response at the scale of the individual rod, as the proteins of the capsid could change their folding somewhat in response to shifting salt concentrations in a way that cannot be expected from crystalline cellulose nanorods. Thus, this may be a case in which a comparison between the two systems is inappropriate.

Dried CNC films

Dried CNC films with a helical internal structure are invariably produced by depositing a suspension onto a substrate, for example, by drop casting or spin coating, and then removing the water by drying. During the drying process, the suspension will decrease in volume and eventually reach a stage where the rod-like CNC particles are locked in place in a glass-like state, with an arrangement that can be amorphous or ordered depending on the history as well as the properties of the suspension. The drying rate is controlled by the sample's geometry, the partial pressure of water in the atmosphere and the temperature.

The drying process can be subdivided into several steps.[56,69] At the initial stage, when the sample is fluid throughout, the surface of the suspension is always wet because water flows from the interior to the surface. The volume fraction of particles increases continuously with the evaporation of solvent until the particles touch each other and no substantial further shrinkage can take place. At this critical point, which can occur at low volume fractions in the case of rod-like particles such as CNCs, the liquid-vapor interface of water starts to recede into the pores of the body, and the drying rate decreases significantly as the transport of water to the surface of the body becomes rate-limiting.

Removing solvent from a colloidal suspension by evaporation is thus a critical process that can result in the arrest of various nonequilibrium states and can also induce significant heterogeneities as the drying front passes over the film.[70–75] It is therefore not surprising that evaporative drying of dilute CNC dispersions spread on a wetting substrate normally results in inhomogeneous films. Several examples can be found in the literature,[15,29] and in the inset of Figure 5d, a film prepared by drying a 4.8 wt% wood-derived CNC suspension is shown. It has a characteristic texture with radially varying color (the origin of the color will be discussed below). A close-up of the microscope image (the main photos in Figures 5b–d) reveals that the film features quite widely spaced parallel lines, indicating the formation of a helix in the plane of the film with a long pitch.

Majoinen *et al.*[29] recently published scanning electron microscopy images of fractured dried CNC films; they found left-handed helical rod arrangements with p in the range of 2–6 μm. The strong variation of p that they reported from the same sample suggests that the observed helical arrangements are nonequilibrium glassy states, arrested at different stages of solvent evaporation and thus with a different pitch in different domains. They correctly noted that a helix with p in the range of several microns cannot give rise to visible Bragg reflection. However, their alternative explanation—that colors from CNC films would arise from birefringence-driven interference effects—leaves colors observed by the naked eye (without polarizers), as shown in the inset in Figure 5d, a mystery because birefringence colors are only visible between crossed polarizers (see Supplementary Box 2).

The colors in Figure 5b are in fact primarily due to visible Bragg reflection, or a photonic bandgap, originating from the helical nanorod arrangement, as confirmed in Figures 5c and d by demonstrating that the light is circularly polarized with the same handedness as the CNC helix (see Supplementary Box 2). The same conclusion was drawn by several other research groups, some of whom followed the more complex course of action to measure the circular dichroism in order to demonstrate the handedness.[15,21,63,76] It is important to remember that Bragg reflection does not occur for light that is incident perpendicular to the helix; the light needs to enter essentially along the helix axis to experience the photonic bandgap. Furthermore, p must be quite close to the wavelength of light within the film, with the allowed offset given by the angle of incidence according to Bragg's law (see Supplementary Box 2). The fact that we see iridescent colors thus tells us that the sample must have a helical arrangement essentially along the film normal, and the pitch must be on the order of a few hundred nanometers. However, we clearly see that the texture is rich in parallel lines with a distance on the order of 1–10 μm, suggesting a helix with a pitch one or two orders of magnitude too large for visible Bragg reflection (see Supplementary Box 1). In addition, the axis of the helix giving rise to this textural feature lies in the film plane instead of perpendicular to it; hence, it has the wrong geometry. The pitch measured in the fluid state has never been reported to be below 1 μm; thus, it seems that no equilibrium liquid crystalline CNC phase could give rise to iridescence.

These intriguing superposed phenomena and apparent contradictions regarding the phase behavior of fluid suspensions and dried samples must be further investigated and clarified to enable better control of the helical pitch and obtain more uniform samples. There is a strong need for experiments using synchronized complementary

techniques, for example, electron microscopy on specific areas of samples that have been previously characterized carefully by polarizing microscopy, with care being taken to record precise information about the sample orientation and location throughout the process. To stimulate further research into the matter, we here propose a tentative explanation to the observations discussed above, taking as a starting point the possibility of a glass transition that takes place nonuniformly within the film. We limit ourselves to the case of a suspension that is initially fully liquid crystalline, as the presence of an interphase boundary in suspensions that are initially in the phase coexistence regime may significantly complicate the process.

It is plausible that the first part of the sample to enter a glassy state is close to the liquid-vapor interface, where the CNC concentration increases rapidly as the water evaporates. Judging from the textural evidence (for example, Figures 5b and c), there are regimes slightly below the surface where the helix has developed in the plane of the film, with p in the range of tens of microns (a lying helix is unlikely at the surface because the interface with air strongly favors a specific CNC rod orientation, generally parallel to the surface). These regimes are locked in this state by the glass formation, but further into the bulk, the sample is still in a liquid crystalline state. To reach the glass transition threshold there, water must diffuse to the surface, where it can evaporate. However, diffusion slows dramatically because the surface regime has been vitrified, as discussed above; hence, the increase in bulk concentration is much slower than at the surface, delaying the gelation in the core of the film, just as the glass transition in the case of a polymer melt is delayed by cooling very slowly. In the bulk, the CNC concentration could thus have the chance to increase further before the glass transition, yielding a sufficiently short pitch to produce a photonic bandgap in the visible wavelength range. The bulk helix also appears to be oriented more or less along the film normal; otherwise, no colors could be generated. This conjecture would have to be corroborated with careful electron microscopy investigations of dried and optically characterized CNC films as a function of depth and perhaps also by *in situ* studies of the local ordering using, for example, microfocus small angle X-ray scattering during drying.

It is important to note that the formation of equilibrium structures over large distances can be a very slow process in lyotropic liquid crystals. In their study of cholesteric helix formation in *fd* virus suspensions at varying ionic strength, Kang and Dhont[77] found that it can take up to 100 h to develop the helix, even for a low-viscosity suspension. If gelation occurs on a time scale shorter than the time required to reach the equilibrium helical superstructure, a state that appears to be non-helical may result, but this is then a nonequilibrium glassy state that is not representative of the relaxed cholesteric phase. This scenario is quite likely for low salt suspensions of bacterial CNCs, as their high aspect ratio leads to a high suspension viscosity even at low CNC concentrations. This will promote gelation while simultaneously counteracting twisting.[64] The stabilization of a helix tight enough to show visible lines could thus require a very long equilibration time, as well as a high concentration of CNCs (the CNC is the only chiral species and hence the source of the twisting). Thus, there is a substantial risk of arrest in a glassy state before the helix has time to fully develop. It is clear that more studies of this critical transition state are needed.

TOWARD STRUCTURE CONTROL AND APPLICATIONS OF SELF-ASSEMBLED CNCs

Orienting the director or helix axis

One aspect of thermotropic liquid crystals that has been key to their immense success in display devices is the ease in controlling the steady-state director orientation by a specially prepared alignment surface and reorienting it dynamically by the application of an electric field. For the commercial application of CNCs in various situations, it would be desirable if similar control of the nanorod orientation could be achieved. The alignment surfaces developed for display devices generally cannot be used for lyotropic liquid crystals, and it is thus unlikely that the CNC orientation can be influenced by them. It does not seem unreasonable, however, that an appropriately nanostructured surface (typically with parallel ridges with a pitch on the order of the CNC rod diameter) could work as an aligning substrate. An alternative to topological patterning of the aligning substrate could be to produce surfaces with a linear array of hydrophobic/hydrophilic or cationic/anionic surface chemistry, with a pitch adapted to the size of the CNC nanorods.

To date, attempts to control the CNC director orientation have focused on the use of external fields, mechanical (shearing), electrical or magnetic, all with some degree of success. The only technique reported thus far to be capable of controlling the direction of the cholesteric helix is magnetic field application. This technique works because CNCs have a negative diamagnetic anisotropy,[78,79] that is, the rods align perpendicular to the magnetic field.[20] Because the rods of a cholesteric CNC suspension are all perpendicular to the helix axis, a cholesteric CNC suspension placed in a sufficiently strong magnetic field will have its helix uniformly aligned along the field direction. This has been experimentally confirmed by Revol *et al.*[37] and Kimura *et al.*[80] The latter team found that the application of a moderate field of 1 T over a few hours can give good results. The procedure should work best for suspensions toward the low-concentration side of the cholesteric regime, which minimizes the viscosity. By starting with a relatively low CNC concentration and evaporating the solvent slowly in a uniform magnetic field, it is thus possible to produce films with uniformly oriented helices.

The dielectric anisotropy of CNCs is positive, and an electric field thus acts to unwind the helix. Habibi *et al.*[81] demonstrated uniform CNC alignment in films obtained by drying CNC suspensions in the presence of electric fields with frequencies in the kHz–MHz range and an amplitude of $\sim 2\,\mathrm{kV\,cm^{-1}}$. Additionally, shear flow will generally induce uniaxial CNC alignment, that is, it provides another means of unwinding the helix. Films with uniform nanorod alignment achieved by shearing were reported by Hoeger *et al.*[82] An X-ray study of the alignment of a liquid crystalline CNC suspension under shear flow with varying shear rates conducted by Ebeling *et al.*[83] indicated quite complex behavior, with very different results depending on the shear rate. Further investigation of the impact of shear flow on cholesteric CNC suspensions, in particular using optical methods (which give more direct information about helical superstructures), should be conducted. By drying films with varying starting concentrations under continuous shear flow, it may be possible to obtain dried films with interesting internal structures.

Using CNC suspensions to produce chiral hybrids and templated materials

Cholesteric CNC suspensions have recently been used as templates to produce inorganic films with an internal left-handed helical structure.[21,76,84–86] MacLachlan and co-workers produced CNC-templated films by adding inorganic sol-gel precursors such as tetramethylorthosilicate or 1,2-bis(trimethoxysilyl)ethane and simply allowing a certain amount of the suspension to dry under ambient conditions in a Petri dish. The CNC self-assembles into a cholesteric phase as the concentration increases in the precursor solution, and the resulting film after solidification and calcination or acid treatment

obtains an internal structure that is a replica of the CNC helix. The key ideas for this type of templating approach and a comparison to ordinary drying of CNC suspensions are schematically summarized in Figure 6.

Generally, the helical pitch of the CNC-inorganic composite before calcination is larger than visible light wavelengths, and the initial composite film therefore shows no color. However, after the cellulose has been removed, the remaining inorganic film frequently shows visible Bragg reflection and the resulting characteristic iridescent colors. Scanning electron microscopy investigations in these cases revealed that the removal of the CNCs leads to a compression of the helical structure such that the periodicity is small enough that the photonic bandgap falls within the visible range.

Films templated from CNCs are attractive because they combine the high surface area of mesoporous materials with the long-range ordering of liquid crystals, specifically with the helical arrangement of the chiral nematic phase. Following the approach of the MacLachlan team, one can thus endow any inorganic material that can be templated from a CNC suspension with photonic crystal properties, with visible Bragg reflection if the pitch is in the range of a few hundred nm. At the same time, the material may exhibit excellent catalytic properties. Thus far, helical silica,[21] organosilica,[85] TiO_2,[84] a metal nitride/carbon composite[87] and carbon[86] have been produced in this way.

The templating strategy offers more than simply transferring the helical structure to different materials. In fact, the optical response of the inorganic replica can differ from that of a pure dried CNC film in some important ways. While the latter has a continuously varying refractive index due to the rotation of the birefringent CNC rods, a templated amorphous inorganic film has a repeated discrete contrast between the refractive index of air and the single refractive index of the optically isotropic amorphous inorganic material. Therefore, the reflection can be turned off by filling the voids with an index matching fluid[21,85] and turned on again by evaporating the liquid. If the voids were instead filled with a thermotropic nematic, where the refractive index for the orientation in the absence of a field matches that of the inorganic material, this switching could be very rapid and reversible. By applying an electric field, the thermotropic nematic would reorient such that the index matching is lost, and the film would appear colored. Although the original dried CNC film is also porous, such an ON/OFF switching of its photonic crystal properties is not possible because no index matching fluid exists for a matrix material that is itself birefringent. It is also likely that not only the helix periodicity but also the thicknesses of the inorganic and air layers and their sum (which gives the local optical period), compared with visible light wavelengths, are very important for the generated colors.

An attractive potential application of transparent CNC-templated inorganic materials that has not yet been discussed is cholesteric-based mirrorless lasing.[88,89] Recent work by Takezoe and co-workers [90,91] has demonstrated that the combination of solidified cholesteric liquid crystal films with different pitch values with an intermediate film of non-chiral low molar mass nematic can produce broadband (essentially white light) cavity mode lasing with tunability offered by the switchable nematic layer. Moreover, the combination of multiple solidified cholesteric layers can reduce the lasing threshold dramatically.[92] These studies were performed with reactive thermotropic mesogens that were polymerized into a solid film after the cholesteric structure with the desired pitch had formed. While this is an appropriate strategy in some cases, replacing the organic film

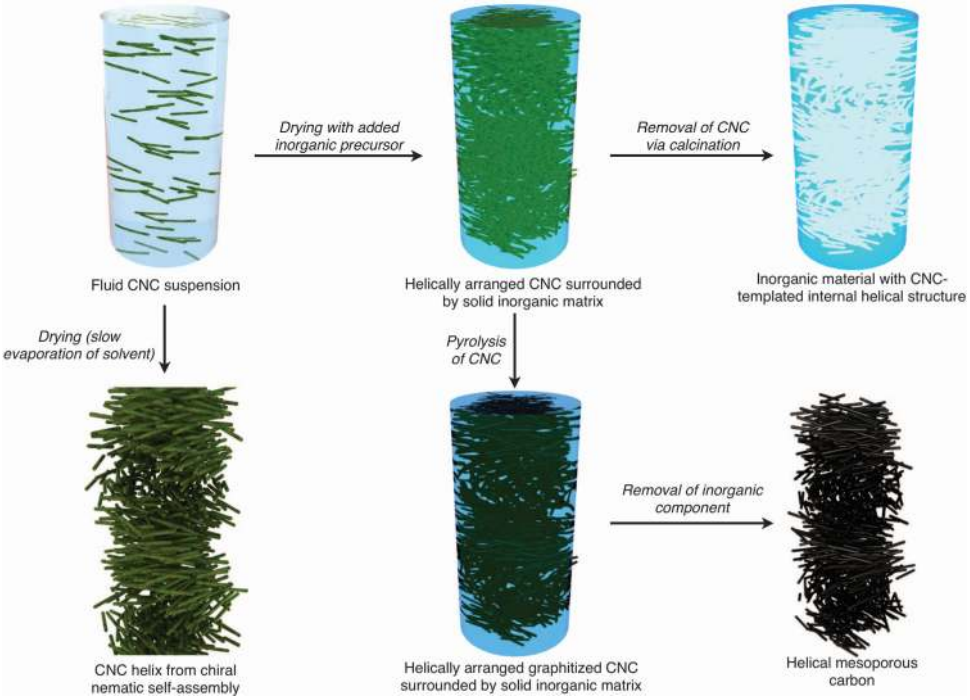

Figure 6 Schematic illustration of the CNC-templating of inorganic materials (as explored by MacLachlan and co-workers[21,76,84–86]) compared with the preparation of dried CNC films. The starting point is always a fluid CNC suspension (top left), which may be liquid crystalline or isotropic. By drying this without additives, a dried film with left-handed, helically arranged CNC rods is produced (bottom left). If an inorganic precursor is added before drying, the CNC helix is contained in an inorganic solid matrix (top middle). By calcinating the sample, the CNCs are removed, leaving the inorganic material with a CNC-templated internal helical structure (top right). If, instead, the CNCs are pyrolyzed into carbon (downwards track, middle) followed by the removal of the inorganic component, a helically arranged mesoporous carbon structure results (bottom right).

with an inorganic one that has been templated from CNC may have substantial advantages in lasing applications, particularly regarding the device lifetime, which is always an issue when organic materials are exposed to high-intensity light.

CNC-templated mesoporous carbon does not feature attractive photonic crystal properties because carbon absorbs too strongly across the visible wavelength range. However, helically templated carbon has many other attractive properties, suggesting its potential applications in supercapacitors (large surface area), transistors and sensors (semiconducting behavior of the mesoporous carbon) or chirality detectors/purifiers (enantioselective adsorption).[86]

CONCLUDING REMARKS AND OUTLOOK

The study of CNCs and their suspensions is a fascinating research field that has attracted significant interest, largely because of the potential of CNCs to be used as a renewable nanomaterial (that is, a material with nanoscale features that is sustainably produced from natural resources) with the capacity for self-assembly. Nanostructured films with a photonic band gap arising from the spontaneous helix formation in the cholesteric liquid crystal phase of CNC suspensions have been the focus of several studies. The use of a CNC suspension as a self-assembled template for the synthesis of inorganic materials that adopt the CNC-derived periodic internal structure offers a promising and versatile platform for fabricating multifunctional mesoporous materials with photonic crystal properties and very large surface areas. The introduction of other inorganic materials with higher refractive indices may be particularly attractive for photonic devices such as tunable mirrorless lasers, and CNC-templated materials with specific surface functionalities may open the way for the development of enantioselective sensors. Moreover, a similar templating route could be used to produce strong and fracture-resistant composites (Figure 7), with a helical internal structure derived from CNC, that mimic high-performance biomaterials such as lobster cuticle.[22,23]

Fundamental issues related to the sensitive balance between liquid crystal formation and gelation/glass formation—two processes that are both promoted by the high aspect ratio of CNC rods—have yet to be fully understood. In particular, when cholesteric structures with a short and highly specified pitch are desired, primarily for photonic devices, one must develop a means of handling the transition into a

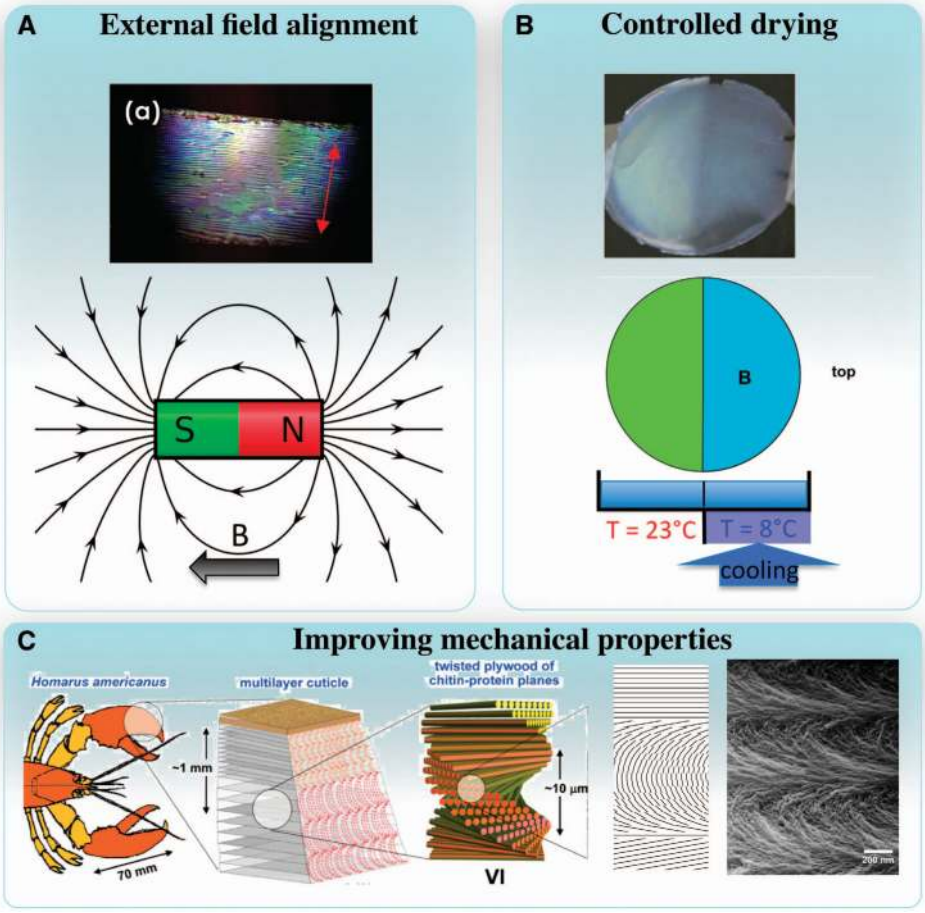

Figure 7 Overview of some promising directions for future research on and applications of liquid crystalline CNC suspensions. (**A**) Alignment by external field application; (a) crossed polarizer image of an aligned fingerprint texture after a vertical magnetic field treatment (ca. 10 T) for ca. 50 h. Reprinted with permission from Kimura *et al.*[80] Copyright (2005) American Chemical Society. (**B**) Pattern formation in a CNC film produced by maintaining the two halves of the Petri dish at different temperatures during cooling. Reproduced with permission from Beck *et al.*,[61] Copyright (2013) Springer. (**C**) Enhanced mechanical properties arising from a hierarchical ordering of building blocks arranged in a helical fashion, giving composites the ability to accommodate loadings at different scales, as exemplified by lobster cuticle, which contains the CNC analog chitin in a composite with proteins. Reproduced with permission from Nikolov *et al.*,[22] Copyright © 2010 WILEY-VCH Verlag GmbH & Co. KGaA, Weinheim. The characteristic Bouligand arcs (black and white drawing following[23]), resulting from an oblique cut through the helical structure, can be found in the lobster cuticle as well as in the dried CNCs (right image, reproduced with permission from Terpstra *et al.*,[95] The Royal Society of Chemistry).

nonequilibrium glassy state, as this becomes increasingly likely at the high CNC concentrations required for a short-pitch helix. To this end, controlled drying (Figure 7) and alternative solvent removal strategies are of interest. Another possible approach to improving the control of the helical self-assembly could be to vary the atmospheric humidity during evaporation or to add a nonvolatile co-solvent.[72]

The possibility of controlling the alignment of CNCs, in helical or non-helical states, also deserves more attention. Large-scale uniform alignment with control of the director and/or helix axis orientation has been made possible by using appropriately designed nano patterned substrates and/or subjecting the drying CNC suspension to appropriately selected mechanical, electrical or magnetic fields. Such control is a requirement for several applications such as lasers, security papers and certain sensors. Likewise, attempts to reduce the length distribution of CNCs could be very rewarding, as this could lead not only to the appearance of smectic and/or columnar phases of CNCs, which are of fundamental interest, but also to other applications in nanostructured and ordered composite materials. Many analogies can be drawn with other liquid crystalline colloidal suspensions, from rod-shaped viruses, mineral nanorods or carbon nanotubes, thus aiding the understanding of the behavior of CNCs.

CONFLICT OF INTEREST

The authors declare no conflict of interest.

ACKNOWLEDGEMENTS

Financial support from STINT (Sweden) and the National Research Foundation (Korea, grant number 490-20110031) is gratefully acknowledged. LB, MS and CS acknowledge the Wallenberg Wood Science Center and the Knut and Alice Wallenberg Foundation for partial funding. LB also acknowledges the Humboldt Foundation for financial support.

1 Fratzl, P. Biomimetic materials research: what can we really learn from nature's structural materials? *J. R. Soc. Interface* **4,** 637–642 (2007).
2 Wicklein, B. & Salazar-Alvarez, G. Functional hybrids based on biogenic nanofibrils and inorganic nanomaterials. *J. Mater. Chem. A* **1,** 5469–5478 (2013).
3 Pennisi, E. Diverse crystals account for beetle sheen. *Science* **341,** 120 (2013).
4 Yang, W., Chen, I. H., Gludovatz, B., Zimmermann, E. A., Ritchie, R. O. & Meyers, M. A. Natural flexible dermal armor. *Adv. Mater.* **25,** 31–48 (2013).
5 Weaver, J. C., Milliron, G. W., Miserez, A., Evans-Lutterodt, K., Herrera, S., Gallana, I., Mershon, W. J., Swanson, B., Zavattieri, P., DiMasi, E. & Kisailus, D. The stomatopod dactyl club: a formidable damage-tolerant biological hammer. *Science* **336,** 1275–1280 (2012).
6 Matranga, A., Baig, S., Boland, J., Newton, C., Taphouse, T., Wells, G. & Kitson, S. Biomimetic reflectors fabricated using self-organising, self-aligning liquid crystal polymers. *Adv. Mater.* **25,** 520–523 (2013).
7 Studart, A. R. Towards high-performance bioinspired composites. *Adv. Mater.* **24,** 5024–5044 (2012).
8 Omenetto, F. G. & Kaplan, D. L. New opportunities for an ancient material. *Science* **329,** 528–531 (2010).
9 Klemm, D., Kramer, F., Moritz, S., Lindstrom, T., Ankerfors, M., Gray, D. & Dorris, A. Nanocelluloses: a new family of nature-based materials. *Angew. Chem. Int. Edit.* **50,** 5438–5466 (2011).
10 Habibi, Y., Lucia, L. & Rojas, O. J. Cellulose nanocrystals: chemistry, self-assembly, and applications. *Chem. Rev.* **110,** 3479–3500 (2010).
11 Moon, R. J., Martini, A., Nairn, J., Simonsen, J. & Youngblood, J. Cellulose nanomaterials review: structure, properties and nanocomposites. *Chem. Soc. Rev.* **40,** 3941–3994 (2011).
12 Eichhorn, S. J., Dufresne, A., Aranguren, M., Marcovich, N. E., Capadona, J. R., Rowan, S. J., Weder, C., Thielemans, W., Roman, M., Renneckar, S., Gindl, W., Veigel, S., Keckes, J., Yano, H., Abe, K., Nogi, M., Nakagaito, A. N., Mangalam, A., Simonsen, J., Benight, A. S., Bismarck, A., Berglund, L. A. & Peijs, T. Review: current international research into cellulose nanofibres and nanocomposites. *J. Mater. Sci.* **45,** 1–33 (2010).
13 Isogai, A., Saito, T. & Fukuzumi, H. TEMPO-oxidized cellulose nanofibers. *Nanoscale* **3,** 71–85 (2011).
14 Dufresne, A. Comparing the mechanical properties of high performances polymer nanocomposites from biological sources. *J. Nanosci. Nanotechnol.* **6,** 322–330 (2006).
15 Zhang, Y. P., Chodavarapu, V. P., Kirk, A. G. & Andrews, M. P. Nanocrystalline cellulose for covert optical encryption. *Proc. SPIE 8258, Organic Photonic Materials and Devices XIV* **8258,** 825808 (2012).
16 Webster, T. J. Nanotechnology: better materials for all implants. *Mater. Sci. Forum* **539,** 511–516 (2007).
17 Thomas, S. A review of the physical, biological and clinical properties of a bacterial cellulose wound dressing. *J. Wound Care* **17,** 349–352 (2008).
18 Revol, J. F., Bradford, H., Giasson, J., Marchessault, R. H. & Gray, D. G. Helicoidal self-ordering of cellulose microfibrils in aqueous suspension. *Int. J. Biol. Macromol.* **14,** 170–172 (1992).
19 Lagerwall, J. P. F. & Scalia, G. A new era for liquid crystal research: applications of liquid crystals in soft matter nano-, bio- and microtechnology. *Curr. Appl. Phys.* **12,** 1387–1412 (2012).
20 de Gennes, P.-G. & Prost, J. *The Physics of Liquid Crystals* (Clarendon Press, Oxford, UK, 1993).
21 Shopsowitz, K. E., Qi, H., Hamad, W. Y. & MacLachlan, M. J. Free-standing mesoporous silica films with tunable chiral nematic structures. *Nature* **468,** 422–425 (2010).
22 Nikolov, S., Petrov, M., Lymperakis, L., Friák, M., Sachs, C., Fabritius, H., Raabe, D. & Neugebauer, J. Revealing the design principles of high-performance biological composites using ab initio and multiscale simulations: the example of lobster cuticle. *Adv. Mater.* **22,** 519–526 (2010).
23 Bouligand, Y. Liquid crystals and biological morphogenesis: ancient and new questions. *C. R. Chim.* **11,** 281–296 (2008).
24 Bouligand, Y. The renewal of ideas about biomineralisations. *Comptes Rendus-Palevol* **3,** 617–628 (2004).
25 Besseau, L. & Bouligand, Y. The twisted collagen network of the box-fish scutes. *Tissue Cell* **30,** 251–260 (1998).
26 Bouligand, Y. Defects and textures in cholesteric analogues given by some biological systems. *J. Phys. Colloque* **36,** 331–336 (1975).
27 Bouligand, Y. Sur l'existence de' pseudomorphoses cholestériques' chez divers organismes vivants. *J. Phys. Colloque* **30,** 90–103 (1969).
28 Kim, S.-H., Lee, S. Y., Yang, S.-M. & Yi, G.-R. Self-assembled colloidal structures for photonics. *NPG Asia Mater* **3,** 25–33 (2011).
29 Majoinen, J., Kontturi, E., Ikkala, O. & Gray, D. G. SEM imaging of chiral nematic films cast from cellulose nanocrystal suspensions. *Cellulose* **19,** 1599–1605 (2012).
30 Hirai, A., Inui, O., Horii, F. & Tsuji, M. Phase separation behavior in aqueous suspensions of bacterial cellulose nanocrystals prepared by sulfuric acid treatment. *Langmuir* **25,** 497–502 (2009).
31 Sahimi, M. & Arbabi, S. Mechanics of disordered solids. II. Percolation on elastic networks with bond-bending forces. *Phys. Rev. B* **47,** 703–712 (1993).
32 Hough, L., Islam, M., Janmey, P. & Yodh, A. Viscoelasticity of single wall carbon nanotube suspensions. *Phys. Rev. Lett.* **93,** 168102 (2004).
33 Hubbe, M. A., Rojas, O. J., Lucia, L. A. & Sain, M. Cellulosic nanocomposites: a review. *BioResources* **3,** 929–980 (2008).
34 Siró, I. & Plackett, D. Microfibrillated cellulose and new nanocomposite materials: a review. *Cellulose* **17,** 459–494 (2010).
35 Rånby, B. G. Aqueous colloidal solutions of cellulose micelles. *Acta Chem. Scand.* **3,** 649–650 (1949).
36 Araki, J., Wada, M., Kuga, S. & Okano, T. Flow properties of microcrystalline cellulose suspension prepared by acid treatment of native cellulose. *Colloid Surf. A* **142,** 75–82 (1998).
37 Revol, J. F., Godbout, L., Dong, X. M., Gray, D. G., Chanzy, H. & Maret, G. Chiral nematic suspensions of cellulose crystallites - phase-separation and magnetic-field orientation. *Liq. Cryst.* **16,** 127–134 (1994).
38 Salajkova, M., Berglund, L. A. & Zhou, Q. Hydrophobic cellulose nanocrystals modified with quaternary ammonium salts. *J. Mater. Chem.* **22,** 19798–19805 (2012).
39 Araki, J., Wada, M. & Kuga, S. Steric stabilization of a cellulose microcrystal suspension by poly (ethylene glycol) grafting. *Langmuir* **17,** 21–27 (2001).
40 Hasani, M., Cranston, E. D., Westman, G. & Gray, D. G. Cationic surface functionalization of cellulose nanocrystals. *Soft Matter* **4,** 2238–2244 (2008).
41 Bates, M. A. & Frenkel, D. Influence of polydispersity on the phase behavior of colloidal liquid crystals: A Monte Carlo simulation study. *J. Chem. Phys.* **109,** 6193–6199 (1998).
42 Bolhuis, P. & Frenkel, D. Tracing the phase boundaries of hard spherocylinders. *J. Chem. Phys.* **106,** 666–687 (1997).
43 Kang, K. & Dhont, J. K. G. Structural arrest and texture dynamics in suspensions of charged colloidal rods. *Soft Matter* **9,** 4401–4411 (2013).
44 Grelet, E. Hexagonal order in crystalline and columnar phases of hard rods. *Phys. Rev. Lett.* **100,** 168301 (2008).
45 Dogic, Z. & Fraden, S. Ordered phases of filamentous viruses. *Curr. Opin. Colloid Interface Sci.* **11,** 47–55 (2006).
46 Vroege, G. J., Thies-Weesie, D. M. E., Petukhov, A. V., Lemaire, B. J. & Davidson, P. Smectic liquid-crystalline order in suspensions of highly polydisperse goethite nanorods. *Adv. Mater.* **18,** 2565–2568 (2006).
47 Puech, N., Blanc, C., Grelet, E., Zamora-Ledezma, C., Maugey, M., Zakri, C., Anglaret, E. & Poulin, P. Highly ordered carbon nanotube nematic liquid crystals. *J. Phys. Chem. C* **115,** 3272–3278 (2011).
48 Ao, G. Y., Nepal, D., Aono, M. & Davis, V. A. Cholesteric and nematic liquid crystalline phase behavior of double-stranded dna stabilized single-walled carbon nanotube dispersions. *ACS Nano* **5,** 1450–1458 (2011).

49 Zamora-Ledezma, C., Blanc, C., Maugey, M., Zakri, C., Poulin, P. & Anglaret, E. Anisotropic thin films of single-wall carbon nanotubes from aligned lyotropic nematic suspensions. *Nano Lett.* **8,** 4103–4107 (2008).
50 Song, W. H., Kinloch, I. A. & Windle, A. H. Nematic liquid crystallinity of multiwall carbon nanotubes. *Science* **302,** 1363–1363 (2003).
51 Onsager, L. The effects of shape on the interaction of colloidal particles. *Ann. N. Y. Acad Sci.* **51,** 627–659 (1949).
52 Araki, J. & Kuga, S. Effect of trace electrolyte on liquid crystal type of cellulose microcrystals. *Langmuir* **17,** 4493–4496 (2001).
53 Gebauer, D., Oliynyk, V., Salajkova, M., Sort, J., Zhou, Q., Bergström, L. & Salazar-Alvarez, G. A transparent hybrid of nanocrystalline cellulose and amorphous calcium carbonate nanoparticles. *Nanoscale* **3,** 3563–3566 (2011).
54 Dong, X. M., Revol, J. F. & Gray, D. G. Effect of microcrystallite preparation conditions on the formation of colloid crystals of cellulose. *Cellulose* **5,** 19–32 (1998).
55 Dong, X. M., Kimura, T., Revol, J. F. & Gray, D. G. Effects of ionic strength on the isotropic-chiral nematic phase transition of suspensions of cellulose crystallites. *Langmuir.* **12,** 2076–2082 (1996).
56 Hunter, R. J. *Foundations of Colloid Science* (Oxford University Press, Cary, NC, USA, 2001).
57 Stroobants, A., Lekkerkerker, H. N. W. & Odijk, T. Effect of electrostatic interaction on the liquid crystal phase transition in solutions of rodlike polyelectrolytes. *Macromolecules* **19,** 2232–2238 (1986).
58 van der Schoot, P. P. A. M in *Supramolecular Polymers* (ed Ciferri, A.) 77–106 (Taylor & Francis, Boca Raton, FL, USA, 2005).
59 Turner, M. & Cates, M. Flow-induced phase-transitions in rod-like micelles. *J. Phys.-Condens. Mat.* **4,** 3719–3741 (1992).
60 Schymura, S., Dölle, S., Yamamoto, J. & Lagerwall, J. Filament formation in carbon nanotube-doped lyotropic liquid crystals. *Soft Matter* **7,** 2663–2667 (2011).
61 Beck, S., Bouchard, J., Chauve, G. & Berry, R. Controlled production of patterns in iridescent solid films of cellulose nanocrystals. *Cellulose* **20,** 1401–1411 (2013).
62 Beck, S., Bouchard, J. & Berry, R. Controlling the reflection wavelength of iridescent solid films of nanocrystalline cellulose. *Biomacromolecules* **12,** 167–172 (2011).
63 Pan, J. H., Hamad, W. & Straus, S. K. Parameters affecting the chiral nematic phase of nanocrystalline cellulose films. *Macromolecules* **43,** 3851–3858 (2010).
64 Beck-Candanedo, S., Roman, M. & Gray, D. Effect of reaction conditions on the properties and behavior of wood cellulose nanocrystal suspensions. *Biomacromolecules* **6,** 1048–1054 (2005).
65 Dogic, Z. & Fraden, S. Cholesteric phase in virus suspensions. *Langmuir* **16,** 7820–7824 (2000).
66 Yarovoy, Y. & Labes, M. M. Effect of chiral polymers on lyotropic liquid crystals. *J. Am. Chem. Soc.* **119,** 12109–12113 (1997).
67 Figgemeier, E. & Hiltrop, K. Quantified chirality, molecular similarity, and helical twisting power in lyotropic chiral nematic guest/host systems. *Liq. Cryst.* **26,** 1301–1305 (1999).
68 Dawin, U. C., Dilger, H., Roduner, E., Scheuermann, R., Stoykov, A. & Giesselmann, F. Chirale Induktion in lyotropen Flüssigkristallen: Erkenntnisse zum Einfluss von Lokalisation und Dynamik des Dotierstoffes. *Angew. Chem. Int. Ed.* **122,** 2477–2480 (2010).
69 Ring, T. A. *Fundamentals of Ceramic Powder Processing and Synthesis* (Academic Press, London, UK, 1996).
70 Uetani, K. & Yano, H. Self-organizing capacity of nanocelluloses via droplet evaporation. *Soft Matter* **9,** 3396–3401 (2013).
71 Han, W. & Lin, Z. Learning from 'coffee rings': ordered structures enabled by controlled evaporative self-assembly. *Angew. Chem. Int. Ed.* **51,** 1534–1546 (2012).
72 Zhang, Y., Yang, S., Chen, L. & Evans, J. R. G. Shape changes during the drying of droplets of suspensions. *Langmuir* **24,** 3752–3758 (2008).
73 Hu, H. & Larson, R. G. Marangoni effect reverses coffee-ring depositions. *J. Phys. Chem. B* **110,** 7090–7094 (2006).
74 Rabani, E., Reichman, D. R., Geissler, P. L. & Brus, L. E. Drying-mediated self-assembly of nanoparticles. *Nature* **426,** 271–274 (2003).
75 Deegan, R. D., Bakajin, O., Dupont, T. F., Huber, G., Nagel, S. R. & Witten, T. A. Capillary flow as the cause of ring stains from dried liquid drops. *Nature* **389,** 827–829 (1997).
76 Kelly, J. A., Shopsowitz, K. E., Ahn, J. M., Hamad, W. Y. & MacLachlan, M. J. Chiral nematic stained glass: controlling the optical properties of nanocrystalline cellulose-templated materials. *Langmuir* **28,** 17256–17262 (2012).
77 Kang, K. & Dhont, J. K. G. Glass transition in suspensions of charged rods: structural arrest and texture dynamics. *Phys. Rev. Lett.* **110,** 015901 (2013).
78 Cranston, E. & Gray, D. Formation of cellulose-based electrostatic layer-by-layer films in a magnetic field. *Sci. Technol. Adv. Mat.* **7,** 319–321 (2006).
79 Sugiyama, J., Chanzy, H. & Maret, G. Orientation of cellulose microcrystals by strong magnetic fields. *Macromolecules* **25,** 4232–4234 (1992).
80 Kimura, F., Kimura, T., Tamura, M., Hirai, A., Ikuno, M. & Horii, F. Magnetic alignment of the chiral nematic phase of a cellulose microfibril suspension. *Langmuir* **21,** 2034–2037 (2005).
81 Habibi, Y., Heim, T. & Douillard, R. AC electric field-assisted assembly and alignment of cellulose nanocrystals. *J. Polym. Sci. B Polym. Phys.* **46,** 1430–1436 (2008).
82 Hoeger, I., Rojas, O. J., Efimenko, K., Velev, O. D. & Kelley, S. S. Ultrathin film coatings of aligned cellulose nanocrystals from a convective-shear assembly system and their surface mechanical properties. *Soft Matter* **7,** 1957–1967 (2011).
83 Ebeling, T., Paillet, M., Borsali, R., Diat, O., Dufresne, A., Cavaille, J. Y. & Chanzy, H. Shear-induced orientation phenomena in suspensions of cellulose microcrystals, revealed by small angle X-ray scattering. *Langmuir* **15,** 6123–6126 (1999).
84 Shopsowitz, K. E., Stahl, A., Hamad, W. Y. & MacLachlan, M. J. Hard templating of nanocrystalline titanium dioxide with chiral nematic ordering. *Angew. Chem. Int. Ed.* **51,** 6886–6890 (2012).
85 Shopsowitz, K. E., Hamad, W. Y. & MacLachlan, M. J. Flexible and iridescent chiral nematic mesoporous organosilica films. *J. Am. Chem. Soc.* **134,** 867–870 (2012).
86 Shopsowitz, K. E., Hamad, W. Y. & MacLachlan, M. J. Chiral nematic mesoporous carbon derived from nanocrystalline cellulose. *Angew. Chem. Int. Ed.* **50,** 10991–10995 (2011).
87 Qi, H., Roy, X., Shopsowitz, K. E., Hui, J K-H & MacLachlan, M. J. Liquid-crystal templating in ammonia: a facile route to micro- and mesoporous metal nitride/carbon composites. *Angew. Chem. Int. Ed.* **49,** 9740–9743 (2010).
88 Finkelmann, H., Kim, S. T., Munoz, A., Palffy-Muhoray, P. & Taheri, B. Tunable mirrorless lasing in cholesteric liquid crystalline elastomers. *Adv. Mater.* **13,** 1069–1072 (2001).
89 Palffy-Muhoray, P., Cao, W., Moreira, M., Taheri, B. & Munoz, A. Photonics and lasing in liquid crystal materials. *Philos. Transact. A Math. Phys. Eng. Sci.* **364,** 2747–2761 (2006).
90 Choi, H., Nishimura, S., Toyooka, T., Ishikawa, K. & Takezoe, H. Analysis of cavity-mode lasing characteristics from a resonator with broadband cholesteric liquid-crystal bragg reflectors. *Adv. Funct. Mater.* **21,** 3430–3438 (2011).
91 Choi, H., Kim, J., Nishimura, S., Toyooka, T., Araoka, F., Ishikawa, K., Wu, J. W. & Takezoe, H. Broadband cavity-mode lasing from dye-doped nematic liquid crystals sandwiched by broadband cholesteric liquid crystal bragg reflectors. *Adv. Mater.* **22,** 2680–2684 (2010).
92 Takanishi, Y., Ohtsuka, Y., Suzaki, G., Nishimura, S. & Takezoe, H. Low threshold lasing from dye-doped cholesteric liquid crystal multi-layered structures. *Opt. Express* **18,** 12909–12914 (2010).
93 Wang, Y. A., Yu, X., Overman, S., Tsuboi, M., Thomas, G. J. J. & Egelman, E. H. The structure of a filamentous bacteriophage. *J. Mol. Biol.* **361,** 209–215 (2006).
94 Dölle, S., Lechner, B.-D., Park, J. H., Schymura, S., Lagerwall, J. P. F. & Scalia, G. Utilizing the Krafft phenomenon to generate ideal micelle-free surfactant-stabilized nanoparticle suspensions. *Angew. Chem. Int. Ed.* **51,** 3254–3257 (2012).
95 Terpstra, A. S., Shopsowitz, K. E., Gregory, C. F., Manning, A. P., Michal, C. A., Hamad, W. Y., Yang, J. & MacLachlan, M. J. Helium ion microscopy: a new tool for imaging novel mesoporous silica and organosilica materials. *Chem. Commun.* **49,** 1645–1647 (2013).
96 Heux, L., Chauve, G. & Bonini, C. Nonflocculating and chiral-nematic self-ordering of cellulose microcrystals suspensions in nonpolar solvents. *Langmuir* **16,** 8210–8212 (2000).
97 Araki, J., Wada, M., Kuga, S. & Okano, T. Influence of surface charge on viscosity behavior of cellulose microcrystal suspension. *J. Wood Sci.* **45,** 258–261 (1999).
98 Angles, M. N. & Dufresne, A. Plasticized starch/tunicin whiskers nanocomposites. 1. Structural analysis. *Macromolecules* **33,** 8344–8353 (2000).
99 Revol, J.-F. On the cross-sectional shape of cellulose crystallites in *Valonia ventricosa*. *Carbohydr. Polym.* **2,** 123–134 (1982).

Supplementary Information accompanies the paper on the NPG Asia Materials website (http://www.nature.com/am)